The Impacts of Increased Heat Stress Events on Wheat Yield under Climate Change in China

Xuan Yang [1, 2], Zhan Tian[3], Laixiang Sun[4, 5, 6], Baode Chen [2], Francesco N. Tubiello[7], Yinlong Xu[8]

1. National Meteorological Centre of China Meteorological Administration, Beijing100081, China

2. Shanghai Typhoon Institute of China Meteorological Administration, Shanghai 200030, China

3. Shanghai Climate Center, Shanghai Meteorological Service, Shanghai 200030, China

4. Department of Geographical Sciences, University of Maryland, College Park, MD 20742, USA

5. International Institute for Applied Systems Analysis (IIASA), A-2361 Laxenburg, Austria

6. School of Finance & Management, SOAS, University of London, London WC1H 0XG, UK

7. Statistics Division, Food and Agriculture Organization of the United Nations (FAO), Rome, Italy

8. Institute of Agro-Environment and Sustainable Development, Chinese Academy of Agricultural Sciences, Beijing, China

Correspondence to: Zhan Tian, E-mail: tianz@lries.ac.cn, Tel: +86-21-54896481, Fax: +86-21-54896465; or Laixiang Sun, Email: LSun123@umd.edu, Tel: +1-301-405-8131, Fax: +1-301-314-9299.

29   **ABSTRACT**

30

31   China is the largest wheat producing country in the world. Wheat is one of the two major

32   staple cereals consumed in the country and about 60% of Chinese population eats the grain

33   daily. To safeguard the production of this important crop, about 85% of wheat areas in the

34   country are under irrigation or high rainfall conditions. However, wheat production in the

35   future will be challenged by the increasing occurrence and magnitude of adverse and extreme

36   weather events. In this paper, we present an analysis that combines outputs from a wide range

37   of General Circulation Models (GCMs) with observational data to produce more detailed

38   projections of local climate suitable for assessing the impact of increasing heat stress events

39   on wheat yield. We run the assessment at 36 representative sites in China using the crop

40   growth model CSM-CropSim Wheat of DSSAT 4.5. The simulations based on historical data

41   show that this model is suitable for quantifying yield damages caused by heat stress. In

42   comparison with the observations of baseline 1996-2005, our simulations for the future

43   indicate that by 2100, the projected increases in heat stress would lead to an ensemble-mean

44   yield reduction of –7.1% (with a probability of 80%) and –17.5% (with a probability of 96%)

45   for winter wheat and spring wheat, respectively, under the irrigated condition. Although such

46   losses can be fully compensated by CO_2 fertilization effect as parameterized in DSSAT 4.5, a

47   great caution is needed in interpreting this fertilization effect because existing crop dynamic

48   models are unable to incorporate the effect of CO_2 acclimation (the growth enhancing effect

49   decreases over time) and other offsetting forces.

50

51   **KEY WORDS:** Extreme weather events; heat stress; probabilistic assessment; wheat yield;

52   climate change, China.

53

1. INTRODUCTION

54

55   China is the largest wheat producing country in the world, with a share of 11% in global

56 wheat areas and 17% in global wheat production during the 2014-2015 marketing year

57 (USDA, 2016).   Wheat is the staple food grain in north China and is eaten in the form of

58 steamed bread and noodles. Chinese government and famers have worked very hard to

59 maintain record or near-record levels of wheat production at about 130 million tons in recent

60 years. However, strong domestic demand for premium quality wheat has continued to result

61 in significant wheat imports at a scale of 2 to 6.8 million tons per year during 2011-2015

62 (FAO- GIEWS, 2016; USDA, 2016).   China's effort to maintain basic self-sufficiency in

63 wheat supply in the future will further face the challenge posed by global warming and the

64 resultant increase in the occurrence and magnitude of adverse and extreme weather events,

65 including heat stress. An improved understanding of this new challenge will be of great

66 importance not only for food security in the country but also for the stability and

67 sustainability of the world's food market.

68   There is a growing body of literature that employs various crop-growing models to

69 simulate the impact of increasing temperature during the growing season on crop production

70 (e.g., Lobell & Asner 2003; You et al. 2009; Asseng et al. 2011, 2015; Liu and Tao 2013;

71 Tao and Zhang 2013; Deryng et al. 2014). However, these studies mostly considered the

72 impact of growing season mean temperature on crop development and yield. Teixeira et al.

73 (2013) construct a daily yield damage intensity factor within a 30-day period centered on

74 flowering to estimate the potential yield damage caused by high daily temperatures. Their

75 damage intensity factor ranges from 0 when daytime temperatures (not maximum) are less

76 than or equal to a crop specific critical temperature and increased linearly to a maximum

77 value of 1 when day temperature reached a limiting upper threshold. The method is attractive

78 in its simplicity, but it cannot account for processes of crop growth and development. In this

79 research we assess the impact of high daily temperatures on wheat growth and development

80 at thirty-six representative observation stations in China (cf. Table S1) and to quantify yield

81 damage caused by heat stress events.

82   The crop growing model employed in this study is the CropSim module in the cropping

2

83 system model (CSM) of the Decision Support System for Agro-technology Transfer (DSSAT)

84 (Jones et al. 2003; Hoogenboom et al. 2010). DSSAT is process-oriented and dynamic. It has

85 been widely used for simulating the collective effects of crop genetics, management practices,

86 and weather and soil conditions on the growth, development, and yield of individual crops for

87 more than 25 different crops in various countries around the world,[1] and recently for

88 assessing the impact of rising seasonal mean temperatures on wheat yield (Asseng et al.

89 2015). The CSM-CropSim has a multiplying algorithm to represent crop's initial response to

90 elevated CO_2, but the algorithm is unable to parameterize the process of CO_2 acclimation, i.e.,

91 the growth enhancing effect of elevated CO_2 decreases over time (Long et al. 2004; Smith

92 and Dukes 2013). We activate this algorithm in our simulations for taking into account the

93 potential CO_2 fertilization effect but with cautions in interpreting the relevant results.

94 To quantify yield damage caused by heat stress events, a challenging issue is how best to

95 combine outputs from a wide range of GCMs with observational data, so as to produce robust

96 future climate data in daily-step for crop impact assessment. Because the current GCMs are

97 incapable of properly simulating daily variation of atmosphere owing to their coarse

98 resolutions, which means that the drivers of local climate variation are not captured (Maurer

99 and Hidalgo 2008), and more importantly, poor representation (e.g., parameterization) of

100 physics, the daily weather output of GCMs should not be used directly as input into the

101 CSM-CropSim simulation model. It was reported that certain distortions in daily weather

102 variability can seriously bias crop model simulations (Semenov and Porter 1995; Baron et al.

103 2005). To address this issue, we employ a pseudo-global warming (PGW) method, in which

104 the climate perturbation (or global warming signal) fields produced by GCMs are

105 superimposed onto observed historical daily weather series at specific locations. With the

106 PGW method, we can obtain a new daily data set that includes the future climate change

107 signals produced from monthly mean data of GCMs' projection, which is widely regarded as

108 being the most reliable so far; and the characteristics of daily weather events under the

109 present-day climate, which is most likely to be preserved in the future. The PGW approach is

---

[1] For an informative review, see Timsina and Humphreys (2006).

110   based on the procedures developed in Schär et al. (1996) and has been adopted in many

111   climate model downscaling studies and applications (Tubiello et al. 2000; Kawase et al. 2009;

112   Rasmussen et al. 2011; Yoshikane et al. 2012; Lauer et al. 2013).

113   In the simulations, we work with 96 climate change scenarios, which are produced by

114   applying the PGW procedure to 30 GCMs under 4 Representative Concentration Pathway

115   (RCP) scenarios in the CMIP5 (Phase 5 of Coupled Model Inter-comparison Project) of the

116   IPCC Fifth Assessment Report (cf. Table S2). Wheat growth simulations of the

117   CSM-CropSim Wheat model under these 96 scenarios produce 960 (96×10 years) yield

118   estimations at each station in each focal period. This in turn leads to 960 yield-loss/gain

119   (yield in each scenario minus yield in the baseline) results at each station in each focal period.

120   We use the frequency distribution of these 960 yield-loss/gain results to proxy the probability

121   distribution of yield changes. This naturally leads to a probabilistic assessment of the impact

122   of heat stress events. This probabilistic assessment method is potentially applicable for other

123   crops and in other jurisdictions.

124

2.   MATERIALS AND METHODS

2.1   Study Sites

127   Both winter wheat and spring wheat grow in China, typically in rotation with other crops

128   such as maize and rice. Winter wheat accounts for about 95% of China's total wheat output,

129   with more than 75% of the crop produced in 5 provinces located on the North China Plain,

130   which are Henan, Shandong, Hebei, Anhui, and Jiangsu, in the descending order of output

131   share (FAO- GIEWS, 2016; USDA, 2016). A USDA's estimation indicates that about 85% of

132   wheat areas is under irrigation or high rain-fall conditions (USDA, 2006) and therefore our

133   presentation mainly focuses on the results under the irrigated condition.

134   We selected 36 agro-meteorological observation stations based on the following criterions.

135   They (1) represent the typical cropping system for wheat cultivation in China; (2) differ in

136   terms of geographic and climatologic characteristics; and (3) have over 10 years of records of

137   wheat crop management information and weather data (including planting, anthesis and

138   harvest dates, crop yield, as well as daily records of minimum and maximum temperature,

139 precipitation, and solar radiation). Of these 36 stations, 26 are winter wheat stations and 10

140 are spring wheat stations. General information on the location, climate and wheat cropping

141 calendar at each of these stations is shown in Table S1. The order of stations in all tables and

142 figures of this paper follows the order of planting dates (from the earliest to the latest).

143

144 **2.2 CSM-CropSim Wheat Model**

145   Crop simulation models are designed to assess the impacts of multiple climate factors on

146 crop growth in a way considering how these factors interact with crop growth and yield

147 formation processes that are sensitive to climate. Therefore they are widely employed in

148 climate impact studies in the cropping sector (Challinor et al. 2014; Xiong et al. 2010; Ju et al.

149 2013). We employ the CSM-CropSim Wheat model of the DSSAT V4.5 to assess the impact

150 of climate change and climate variability on wheat development and growth. Similar to other

151 process-oriented crop dynamic models, the CSM-CropSim Wheat calculates daily

152 phenological development (i.e., vegetative growth, flowering, grain growth, maturity and

153 senescence phases) and biomass growth in response to environmental (soil and climate) and

154 management (crop variety, planting conditions, N fertilization, and irrigation) factors. This

155 model is routinely used for quantifying wheat yields under current conditions as well as under

156 climate change scenarios across a wide range of environments in different countries (e.g.,

157 Challinor et al. 2005; Palosuo et al. 2011), including China (e.g., Xiong et al. 2008, 2010).

158   The overall temperature response of the CSM-CropSim wheat model is determined by

159 the integration of a number of individual responses in the wheat growth cycle. Hunt and

160 White (2013) present a technical overview of temperature response settings in the model. Its

161 input files with information on crop management have a section dealing with environmental

162 modifications. This setting allows a user to set up a sequence of simulation runs with the

163 same general management, but with different conditions, for instance different sets of daily

164 maximum and/or minimum air temperatures. Asseng et al. (2015) systematically test 30

165 different wheat crop models of the Agricultural Model Inter-comparison and Improvement

166 Project (AGMIP) against field experiments. The tests are for growing season mean

167 temperatures, which ranged from 15°C to 32°C, including experiments with artificial heating.

168   Their results show that the CSM-CropSim wheat model outperformed other models in terms

169   of simulating anthesis and maturity dates, with an average performance in terms of simulating

170   yield.

171   Elevated CO_2 atmospheric concentrations decrease rates of photorespiration and initially

172   enhance rates of photosynthesis and growth by a significant margin for C3 crops. This effect

173   is represented by a simple multiplying algorithm with regard to the net assimilation rate. The

174   multiplier values changed linearly from 1.0 at 330 ppm CO_2 to 1.25 at 660 ppm CO_2 and then

175   to 1.43 at 990 ppm CO_2 (Hoogenboom et al. 2010). However, now we know that the above

176   initial enhancement effect diminishes over time, a phenomenon known as CO_2 acclimation

177   (Long et al. 2004; Bloom et al. 2010), or can be eliminated by joint water and nitrogen

178   limitation (Reich et al. 2014).[2] The simple multiplying algorithm in CSM-CropSim is unable

179   to capture the effect of this acclimation process and therefore, we must be cautious in

180   interpreting the simulation results on the effect of CO_2 fertilization.

181

182   **2.3 Cultivar Parameters**

183   The crop cultivar parameters, which are named genetic coefficients in DSSAT,

184   quantitatively describe how a particular genotype responds to environmental factors. For

185   example, field experiments reported in Fischer (1985) show a good correlation between

186   kernel number and incident solar radiation in the 30 days preceding anthesis and a

187   proportional relationship between the stem weight at anthesis and the grain number. The

188   CSM-CropSim Wheat model approximates these relationships in mathematical constructs.

189   However, because the exact quantification of the factors determining grain numbers are not

190   well understood, the CSM-CropSim Wheat model needs to calibrate three cultivar

191   coefficients based on field observations of crop growth process to compute grain numbers per

---

[2] Some other forces may also bring in eliminating effects. For example, rising levels of atmospheric CO_2 is highly likely to increase the severity of wheat diseases, thus reducing yields (Váry et al. 2015); and disease levels can become worse when the plants and pathogens have been acclimatized to the higher concentrations of CO_2 beforehand. Furthermore, weeds and other undesirable plants experience CO_2 fertilization as well.

192   plant as determined by the cultivar's genetic potential, canopy weight, average rate of

193   carbohydrate accumulation during flowering, and temperature, water and nitrogen stresses

194   (Jones et al. 2003). These three cultivar coefficients are: G1 or the kernel number coefficient,

195   presented as the number of seeds per unit canopy weight at anthesis (#/g); G2 or the kernel

196   weight coefficient, presented as normal seed weight under optimum conditions (mg); and G3

197   or the spike number coefficient, presented as the normal dry weight (total, including grain) of

198   one unstressed stem at maturity (g). Such coefficient calibration makes the application of the

199   model cultivar- and location-specific, and consequently, the sensitivity results are also

200   cultivar- and location-specific.

201   Calibration of cultivar parameters itself is a knowledge- and technical-demanding work

202   and our calibration for each of the thirty-six stations, which is based on the DSSAT-provided

203   Generalized Likelihood Uncertainty Estimation method, has been published in Tian et al.

204   (2012).

205

206   **2.4 Incorporating Natural Adaptation of the Growing Cycle**

207   We incorporate the natural adaptation of the growing cycle under heat stress in two steps.

208   Simulations in the first step do not alter the sowing dates of the baseline but allow the

209   growing cycle after the sowing dates to follow the growing dynamics specified in the

210   CSM-CropSim wheat model, which means a natural adaptation of the growing cycle to the

211   new weather pattern. In the second step, we extend the natural adaptation simulations to

212   include changes on sowing dates.

213   In the simulations, the irrigated condition means that when the effective water content in

214   the 0-20cm soil layer is below 80% of moisture retention capacity, automatic irrigation set

215   in the model takes place. Other management measures are set at the optimal levels to avoid

216   disturbances caused by variations in management measures.

217

218   **2.5 Dataset**

219   Our analysis of climate change and climate variability is based on the simulations and

220   projections of 30 GCMs used in the CMIP5 for the IPCC Fifth Assessment Report (AR5). In

221   the CMIP5, radiative forcing scenarios are derived from representative concentration

222   pathways (RCPs) (Moss et al. 2010; van Vuuren et al. 2011). Monthly minimum temperature,

223   maximum temperature, precipitation, and solar radiation from historical runs and future

224   scenarios are used and the climate data are obtained from 96 runs of projections for the early

225   century (2016–2025), middle century (2046–2055), and the end of the century (2091–2100)

226   under the RCP scenarios. Table S2 lists the GCMs used in this study, including model

227   resolution, scenarios, and availability. A more detailed documentation of CMIP5 models can

228   be found at http://cmip-pcmdi.llnl.gov/cmip5/.

229   Observed daily data (minimum and maximum temperatures, sunshine hours,

230   precipitation) for the period of 1996-2005, which served as the baseline for the 36 stations,

231   were provided by the Chinese Meteorological Data Center. Solar radiation was estimated

232   using empirical global radiation models based on observed daily sunshine hours (Pohlert,

233   2004). Field data at the study sites, including anthesis and harvest dates, were also provided

234   by the Chinese Meteorological Data Center (Table S1). Soil data were taken from Tian et al.

235   (2012).

236

237   **2.6 PGW Approach**

238   In the PGW approach, the difference between present and future climate conditions

239   simulated by GCMs was chosen to represent the climate warming signal or perturbation. To

240   make the climate warming signal possess as little spatial variation (mostly from weather

241   perturbations) as possible, the decadal climatology is used to average out the weather. The

242   climate perturbation field (climate warming signal) is then added to the current weather field

243   for the selected years, by linearly interpolating from monthly climatologies to each specified

244   time period. In more detail, the climate warming perturbation field is obtained by subtracting

245   the current (1996–2005) monthly 10-yr climatology from a future (2016–2025, 2046–2055,

246   and 2091–2100, respectively) monthly 10-yr climatology, both from the same GCM

247   projection.[3] The climate perturbation field is then added to the current weather field. The

---

[3] For daily data, herein 10 year periods are considered sufficient to generate a climatology. Longer, 20 or 30 year periods should be used to obtain monthly climatologies.

248 difference between climatological fields used here to represent the climate warming signal

249 must have as little spatial variation (mostly from weather perturbations) as possible, so the

250 decadal climatology is used to average out the weather.

251 The signaling variables include minimum temperature, maximum temperature,

252 precipitation, and solar radiation. The new daily data set is obtained by superposing the

253 climate perturbation field to the observed daily data at each of the 36 stations. The

254 superposing is done through linear interpolation from the monthly climatological predictions

255 to each period in the observational daily data, with an assumption that monthly mean is valid

256 on the 16th of each month. The new daily data include the future climate change signals of the

257 GCM perturbation while retaining the characteristics of daily weather events observed in the

258 historical time-series. This was considered to be the most probable distribution in the future

259 based on GCM information. This is because the climate perturbation's primary impact is on

260 the large-scale planetary waves and associated thermodynamics, while the weather patterns

261 entering the domain boundary remained structurally identical in both simulations in terms of

262 frequency and intensity. Weather events can nonetheless evolve within the regional model

263 domain due to altered planetary flow and thermodynamics (Rasmussen et al. 2011).

264

265 **2.7 Definition of Heat Stress in Thermal Sensitive Periods**

266 There is a large body of literature identifying the cardinal temperature thresholds for

267 different phenological processes in wheat under experimental conditions. As summarized in

268 the survey reports of Russell and Wilson (1994) and Porter and Gawith (1999), 31-32°C are

269 commonly regarded as the upper base temperature during the period immediately before

270 anthesis. The official disaster grading standard of China Meteorological Administration

271 (CMA-PAD, 2007) regards 32°C as the upper base temperature for defining heat stress events

272 during the period prior to anthesis in China.

273 We double check the applicability of this official threshold by carrying out the following

274 two sets of tests under the base-line climate. First, we test yield losses caused by imposing a

275 single-day heat stress on the observed anthesis day for the consideration that short periods of

276 heat stress during flowering period cause pollen indehiscence, disrupt pollination, decrease

277   the ability of pollen to germinate, and decrease the rate of pollen tube growth (Jagadish et al.

278   2010; Yadav et al. 2011). Second, we apply the above single-day heat stress event to a period

279   from the 30th day before anthesis to the 6th day after anthesis so as to detect the most sensitive

280   periods before and after anthesis. The results show that grain numbers are significantly

281   reduced as a result of single-day heat in the period spanning from the 20th day before anthesis

282   to the anthesis day, when compared to the impacts prior to this 20-day interval. In contrast,

283   the effect of single-day heat stress on each of the 6 days after anthesis is not significant.

284   These two tests show that the period spanning from the 20th day before anthesis to the

285   anthesis day is the period most sensitive to heat stress featured by the maximum daily

286   temperature exceeding 32°C.

287   For the grain-filling period, the upper base temperature suggested in the literature is

288   between 33.4 and 37.4°C (Russell and Wilson, 1994; Porter and Gawith, 1999). Therefore, it

289   is not a surprise that yield reductions due to single-day heat-stress event above 32°C after

290   anthesis is not significant in our tests. To identify the upper base temperature during the

291   grain-filling period for popular cultivars in China, we test the impact of three consecutive

292   days of heat-stress with maximum daily temperature exceeding 35°C during the grain-filling

293   period. The results indicates that the yield reduction impact of such a heat stress event takes

294   effect about one-week after anthesis, and imposing the same event on later days but before

295   the end of the grain filling period will generate a similar level of damage.

296   Following the above findings, our thermal sensitivity assessments for the future climate

297   conditions will focus on the following two periods: (a) The period spanning from the 20th day

298   before anthesis to the anthesis day, we name it the "pre-anthesis period", in which heat stress

299   occurs if single-day maximum temperature exceeds 32°C. (b) The period spanning from the

300   1st to 20th day after anthesis, we name it the "grain-filling period", in which heat stress occurs

301   when maximum daily temperatures exceed 35°C on three consecutive days.

302

303   **3.   RESULTS**

304   **3.1 Frequency and Intensity of Heat Stress Events**

305   Please note that we work with a set of climate change signaling variables, include

10

306 minimum temperature, maximum temperature, and precipitation, in the CSM-CropSim

307 simulations. Because the ensemble-mean precipitation during the wheat growth season

308 increases, by a moderate or significant scale at all study sites except Longhai, from the

309 baseline of 1996-2005 to 2046-2055 and 2091-2100, and the decreases of precipitation in

310 Longhai are less than 3.4%, as shown in Table S3, our discussion in this paper mainly

311 focuses on the impact of heat stress.

312   Table 1 reports the projected mean increases in the frequency of heat stress occurrence at

313 each of the 36 study sites. It shows that the increases in the frequency of heat stress

314 occurrence during both the pre-anthesis and grain-filling periods at the spring-wheat stations

315 are much more significant than those at the winter-wheat stations. In the pre-anthesis period

316 and compared with the baseline, the ensemble-mean frequency of heat stress occurrence is

317 projected to increase by about 8 (probability: 54%), 12 (70%), and 18 (78%) days/decade by

318 2016-2025, 2046-2055, and 2091-2100, respectively, at the winter-wheat stations. In contrast,

319 the corresponding figures at the spring wheat sites are 30 (60%), 41 (85%), and 55 (88%)

320 days/decade. During the grain-filling period and in comparison with the baseline, the

321 ensemble-mean frequency of heat stress occurrence increases by about 5 (44%), 9 (62%), and

322 15 (70%) days/decade by 2016-2025, 2046-2055, and 2091-2100, respectively, at the

323 winter-wheat stations; and by 22 (58%), 31 (76%), and 44 (83%) days/decade at the

324 spring-wheat sites.

325   To visualize the changes, Figures S2 and S3 depict the time series of the assembled

326 maximum, mean, and minimum of the projected changes in monthly mean (Fig. S2) and

327 maximum (Fig. S3) temperature from the baseline of 1996-2005, for each of the selected nine

328 stations in the wheat production zone of northern China. All these time series show a rising

329 trend. The assembled maximum shows the steepest rise in all stations, which implies (a) an

330 increase in the intensity and (b) an increase in the variability of heat stress. Tables S4 and S5

331 summarize the assembled and decadal mean of the above-mentioned two changes from the

332 baseline of 1996-2005 to each of the three periods: 2016-2025, 2046-2055, and 2091-2100,

333 respectively. They show a trend of increase in both monthly mean and maximum

334 temperatures at all study sites and the probability of such increase is between 92% and 100%.

11

335

336   *(Tables 1, 2 and Figure 1 about here)*

337

3.2 Ensemble Projections of Wheat Yield under the Irrigated Condition

339   Table 2 reports the summary statistics of our simulations in terms of ensemble-mean yield

340   changes, probability of yield change, and standard deviation of yield change relative to the

341   baseline under the irrigated condition. Figure 1 presents the corresponding box plots. Table 2

342   and Figure 1 show that both the extent and probabilities of yield reduction increase with the

343   GCM projected warming trend, at all 36 stations. To put this numerically, the ensemble-mean

344   yield loss in comparison with the baseline will be 4.7 (with a probability of 71%), 5.4 (75%)

345   and 7.1 (80%) percent by 2016-2025, 2046-2055, and 2091-2100, respectively. This suggests

346   an increased risk of reduced yield in the middle and end of this century. In addition, the

347   distributions of yield losses are increasingly skewed to the left when moving from 2016-2025

348   to 2091-2100, as evidenced by the co-increases of the standard deviation and the probability

349   of yield loss in Table 2 and box plots in Figure 1. In contrast to distributions without severe

350   skewness, this high and increasing left-skewness indicates that the increase in standard

351   deviation does not necessarily imply increasing uncertainty in mean yield losses. This finding

352   enriches the existing literature in the climate change impact assessment field.

353   Consistent with the higher sensitivity of spring wheat to heat stress (Tian et al., 2012)

354   and stronger future warming at the spring wheat stations, the yield losses in spring wheat

355   stations are generally more severe than their winter-wheat counterparts in terms of percentage

356   reduction. Spring wheat yield is projected to decrease by 8.2 (with a probability of 93%),

357   12.8 (96%), and 17.5 (96%) percent on average by 2016-2025, 2046-2055, 2091-2100,

358   respectively.

359   There is an increasing body of literature assessing the impact of rising temperatures on

360   wheat production. The most comprehensive one in this literature is Asseng et al. (2015),

361   which systematically tests 30 wheat crop models against field experiments in 30 global

362   locations, with warming signals imposed on growing season mean temperatures. In

363 comparison with their results at two winter wheat stations in China,[4] our results of 7% yield

364 reduction with a standard deviation of 9.6% by the end of the century are in line with the high

365 end of the yield losses in their results under a 2°C increase in seasonal mean temperatures and

366 lower than their results with a 4°C increase in seasonal mean temperatures. In comparison

367 with their results at the only spring wheat station, Harbin, which is located in far north of

368 Northeast China, our results of 17.5% yield reduction with a standard deviation of 14% is in

369 line with their results based on an imposed 4°C increase in seasonal mean temperature.

370

371 **3.3 Natural Adaptation of Crop Growing Cycle**

372   We note that warming would allow for earlier planting of spring wheat and earlier ending

373 of winter wheat dormancy, and this in turn would allow the crop to mature earlier, avoiding

374 heat stress occurred later. Therefore, in our simulations, we allow for the natural adaptation

375 of crop growing cycle to new climate patterns, meaning that the end of dormancy and mature

376 dates will be determined endogenously by the model according to the growth dynamics of the

377 cultivar under the new warming conditions.

378   In addition, we also run simulations on postponing the winter wheat plating dates within

379 a window of 28 days and on bringing forward the spring wheat plating dates within a window

380 of 28 days. The results for winter wheat do not show a statistically significant mitigation

381 effect at virtually all winter wheat stations. The results for spring wheat at the two stations in

382 Xingjian show that about 50-60% of the heat-stress induced yield losses can be avoided by

383 this simple adaptation measure, but the results at other spring wheat stations do not produce

384 statistically significant mitigation effect.

385

386 **3.4 Ensemble Projections of Wheat Yield under the Rain-fed Condition and**

387 **Considering CO$_2$ Fertilization Effect**

388   Although rain-fed wheat production accounts for less than 15% of total wheat production

389 in China (USDA, 2006, 2016) and wheat growth at all 36 study sites are under irrigated

---

[4] They are Luancheng station in Hebei Province of North China Plain and Nanjing station in the lower reach of Yangtze River Basin.

condition, we run simulations at all stations under rain-fed conditions. Table S6 reports the summary statistics of this set of simulations and Figure S4 presents the corresponding box plots. They show that the ensemble-mean yield will increase, in comparison with the baseline, by 7.9, 12.2 and 15.4 percent for winter wheat and by 28.1, 30.3, and 30.5 percent for spring wheat in 2016-2025, 2046-2055, and 2091-2100, respectively. Such increases mainly result from the significant increase in precipitation during the wheat growing season. As reported in Table S3, in comparison with the baseline, the ensemble-mean increases in precipitation during the wheat growing season will be 18.9, 31.6, and 38.5 percent at the 26 winter wheat stations, and 50.1, 78.5, and 74.6 percent at the 10 spring wheat stations by 2016-2025, 2046-2055, and 2091-2100, respectively. However, even the highest yield-increase of 30.5% cannot compete with the gain from irrigation, which typically stands at a level of 75% (USDA, 2006, 2016).

Tables S7 and S8 are the counterparts of Tables 2 and S6, respectively, when considering the CO_2 fertilization effect. Figures S5 and S6 presents the corresponding box plots. Table S7 and Figure S5 indicate that with reference to the baseline, although the incorporation of CO_2 fertilization effect under the irrigated condition cannot reverse the yield losses by 2016-2025, it will result in yield increases by 8.4 and 16.9 percent at winter wheat stations and by 3.4 and 9.3 percent at spring wheat stations by 2046-2055 and 2091-2100, respectively. Under the rain-fed condition, the effect of CO_2 fertilization becomes more significant. The gain on the ensemble-mean yield will be 17.6, 42.5, and 70.2 percent for winter wheat and 39.6, 64.6, and 93.2 percent for spring wheat by 2016-2025, 2046-2055, and 2091-2100, respectively (Table S8 and Figure S6). This means that by the end of this century, the yield gain from the combined effect of increased rainfall and CO_2 fertilization will have the potential to fully match the yield gain from irrigation and thus reduce irrigation water demand. However, as we discussed in Section 2.2, such yield gain could be illusive because the growth enhancing effect of CO_2 decreases over time and the parameterization of DSSAT model is unable to incorporate such acclimation process.

4.   DISCUSSION AND CONCLUSION

419   Wheat is one of the two major staple cereals consumed in China and about 60% of

420   Chinese population eats the grain daily. Basic self-sufficiency of wheat supply in the future

421   will be of fundamental importance not only for food security in China but also for the

422   sustainability of the world's food market. However future wheat production in China will

423   face the challenge posed by the increasing occurrence and magnitude of adverse and extreme

424   weather events such as heat stress. In this research we first combine outputs from a wide

425   range of General Circulation Models (GCMs) with observational data to produce more

426   detailed projections of local climate suitable for assessing the impact of increasing heat stress

427   events on wheat yield. This is done by applying the Pseudo-global Warming Method (PGW)

428   method to the outputs of 96 GCM-RCP combinations to effectively couple observed trend in

429   historical weather fields with the difference components of the global warming signal

430   produced by GCMs. These PGW-enhanced ensembles of climate change scenarios provide a

431   robust way for ensuring a reliable probabilistic assessment of climate change impact on crop

432   yield.

433   We then employ the CSM-CropSim Wheat model of DSSAT 4.5 to simulate wheat

434   development and growth processes under current and future climate conditions at 36

435   representative observation stations in the major wheat growing areas of China. The

436   simulations under current climate conditions indicate that the thermal sensitivity assessments

437   should focus on two critical periods – one spanning from the 20th day preceding flowering to

438   the anthesis day, in which heat stress event occurs if single-day maximum temperature

439   exceeds 32°C; and the other spanning from the 1st to the 20th day after anthesis, in which heat

440   stress events occur if maximum daily temperature exceeds 35°C on three consecutive days.

441   The ensemble of future climate conditions shows increasing frequency and intensity of

442   heat stress incidence. The probability of such increase is also increasing with time. The

443   CSM-CropSim simulations under the 96 climate change scenarios provide a probability

444   assessment of future yield losses caused by heat stress events, which incorporate the natural

445   adaptation of crop growing cycle to new climate conditions.   Our discussion in this

446   concluding section focuses on irrigated wheat production because it accounts for more than

447   85% of the total wheat production in China. The results show ensemble-mean yield

15

448 reductions at all 36 sites, with an increasing trend in terms of both yield reduction extent and

449 the probability of yield reduction. In comparison with the baseline 1996-2005, the extent and

450 probability of yield reduction by 2091-2100 are 7.1% and 80%, respectively, for winter wheat,

451 and 17.5% and 96%, respectively, for spring wheat. The results for winter-wheat are in line

452 with the high end of the yield losses in Asseng et al. (2015) under a 2°C increase in seasonal

453 mean temperatures at Luancheng and Nanjing stations. The results for spring wheat are in

454 line with the results of Asseng et al. (2015) on an imposed 4°C increase in seasonal mean

455 temperature at the Harbin station. Although the CO_2 fertilization effect as parameterized in

456 DSSAT 4.5 can compensate these losses, such fertilization effect might be illusive because

457 the effect of CO_2 acclimation (i.e., the growth enhancing effect decreases over time) and

458 other offsetting forces are not considered in the parameterization of existing crop growth

459 models (Smith and Dukes 2013).

460   Two limitations of this research are worth mentioning. First, despite the advantage of the

461 PGW method in generating coherent and robust scenarios which preserve the characteristics

462 of observed daily weather events while incorporating GCM-derived increases in frequency

463 and intensity, it is unable to consider the nonlinear interaction between climate change and

464 inter-annual variations in regional climate systems. The approach also implies the assumption

465 that the same frequency and intensity of weather perturbations occur in the regional

466 simulation domain for mean conditions of future climate (Rasmussen et al. 2011). These two

467 weaknesses mean that the uncertainty caused by changes in inter annual variability is still not

468 accounted for in the probability assessment of this research. Second, the simulation results

469 from one crop model only are subject to the limitations on thermal-sensitivity in this crop

470 model. As highlighted in Asseng et al. (2013; 2015), a greater proportion of the uncertainty in

471 climate change impact assessments can be attributed to variations across crop models. While

472 the present study enriches the literature by assessing the impact of daily heat stress events

473 under future climate change on wheat growth and development with the assistance of a highly

474 dynamic crop model, future assessments will benefit from extended analyses using multiple

475 crop models.

476

477

478

REFERENCES

479 Asseng S, Foster IAN, Turner NC (2011) The impact of temperature variability on wheat yields.

481 Global Change Biol 17:997-1012. DOI: 10.1111/j.1365-2486.2010.02262.x.

482 Asseng S, Ewert F, Rosenzweig C, et al. (2013) Uncertainty in simulating wheat yields under climate

483 change. Nat Clim Change 3:827–832. DOI: 10.1038/NCLIMATE1916.

484 Asseng S, Ewert F, Martre P, et al. (2015) Rising temperatures reduce global wheat production. Nat

485 Clim Change 5:143-147. DOI: 10.1038/NCLIMATE2470.

486 Baron C, Sultan B, Balme M, et al (2005) From GCM grid cell to agricultural plot: scale issues

487 affecting modelling of climate impact. Philos T R Soc Lond B Biol Sci 360:2095-2108. DOI:

488 10.1098/rstb.2005.1741.

489 Bloom A, Burger M, Asensio J R, Cousins A (2010) Carbon dioxide enrichment inhibits nitrate

490 assimilation in wheat and Arabidopsis. Science 328: 899-901. DOI: 10.1126/science.11864.

491 Challinor A J, Wheeler T R, Craufurd P Q, Slingo J M (2005) Simulation of the impact of high

492 temperature stress on annual crop yields. Agr Forest Meteorol 135:180-189. DOI:

493 10.1016/j.agrformet.2005.11.015.

494 Challinor A J, Watson J, Lobell D B, Howden S M, Smith D R, Chhetri N (2014) A meta-analysis of

495 crop yield under climate change and adaptation. Nature Clim. Change 4:287-291. DOI:

496 10.1038/nclimate2153.

497 CMA-PAD (China Meteorological Administration, Policy and Regulation Department) (2007)

498 Disaster Grading Standard on Dry-hot Wind for Wheat. QX/T 82-2007. Beijing, China

499 Meteorological Press, 547-555. (in Chinese).

500 Deryng D, Conway D, Ramankutty N, Price J, Warren R (2014) Global crop yield response to

501 extreme heat stress under multiple climate change futures. Environ. Res. Lett. 9, 034011 (13pp).

502 DOI: 10.1088/1748-9326/9/3/034011.

503 FAO- GIEWS (2016) GIEWS Country Briefs: China, 22-March-2016. Available at:

504 http://www.fao.org/giews/countrybrief/country.jsp?code=CHN.

505 Fischer RA (1985) Number of kernels in wheat crops and the influence of solar radiation and

506 temperature. J Agr Sciences, 105, 447-462.

507 Hoogenboom G, Jones JW, Wilkens PW, et al. (2010) Decision Support System for Agro-technology

508   Transfer, Version 4.5, Volume 1: Overview. University of Hawaii, Honolulu, USA.

509 Hunt, LA and White JW (2013) The CSM-CROPSIM Wheat model: Temperature responses. In

510   Alderman PD, Quilligan E, Asseng S, Ewert F, and Reynolds MP (Eds), Proceedings of the

511   Workshop on Modeling Wheat Response to High Temperature. CIMMYT, El Batán, Mexico,

512   19-21 June 2013. Mexico, D.F.: CIMMYT.

513 Jagadish SVK, Muthurajan R, Oane R, et al. (2010) Physiological and proteomic approaches to

514   address heat tolerance during anthesis in rice (Oryza sativa L). J Exp Bot 61, 143–156. DOI:

515   10.1093/jxb/erp289.

516 Jones JW, Hoogenboom G. Porter CH, et al. (2003) The DSSAT cropping system model. Europ J

517   Agronomy 18:235-265.

518 Ju H, Lin E, Wheeler T, Challinor A, Jiang S (2013) Climate change modelling and its roles to

519   Chinese crops yield. J Integr Agr 12:892-902. DOI:10.1016/S2095-3119(13)60307-X.

520 Kawase H, Yoshikane T, Hara M, et al. (2009) Intermodel variability of future changes in the

521   Baiurainband estimated by the pseudo global warming downscaling method. J Geophys Res 114

522   (D24). DOI: 10.1029/2009JD011803.

523 Lauer A, Zhang C, Elison-Timm O (2013) Downscaling of climate change in the Hawaii region using

524   CMIP5 results: On the choice of the forcing fields. J Climate 26: 10006-10030. DOI:

525   http://dx.doi.org/10.1175/JCLI-D-13-00126.1.

526 Liu and Tao (2013) Probabilistic change of wheat productivity and water use in China for global mean

527   temperature changes of 1°, 2°, and 3°C. Journal of Applied Meteorology and Climatology, 52,

528   114-129.   DOI: 10.1175/JAMC-D-12-039.1.

529 Lobell DB, Asner GP (2003) Climate and management contributions to recent trends in US

530   agricultural yields. Science, 299, 1032. DOI: 10.1126/science.1078475.

531 Long S P, Ainsworth E A, Rogers A, Ort D R (2004). Rising atmospheric carbon dioxide: plants

532   FACE the future. Annu Rev Plant Biol. 55, 591-628. DOI:

533   10.1146/annurev.arplant.55.031903.141610.

534 Maurer E P, Hidalgo H G (2008) Utility of daily vs. monthly large-scale climate data: an

535   inter-comparison of two statistical downscaling methods. Hydrol. Earth Syst. Sci. 12, 551–563.

536   DOI: 10.5194/hess-12-551-2008.

537   Moss RH, Edmonds JA, Hibbard KA, et al. (2010) The next generation of scenarios for climate

538   change research and assessment. Nature 463:747-756. DOI: 10.1038/nature08823.

539   Palosuo T, Kersebaum KC, Angulo C, et al (2011) Simulation of winter wheat yield and its variability

540   in different climates of Europe: a comparison of eight crop growth models. Eur J

541   Agron 35:103-114. DOI:10.1016/j.eja.2011.05.001.

542   Pohlert T (2004) Use of empirical global radiation models for maize growth simulation. Agr Forest

543   Meteorol 126:47–58. DOI:10.1016/j.agrformet.2004.05.003.

544   Porter J R, Gawith M (1999) Temperatures and the growth and development of wheat: a review,

545   European Journal of Agronomy 10, 23–36. DOI: 10.1016/S1161-0301(98)00047-1.

546   Rasmussen R, Liu C, Ikeda K, et al. (2011) High-resolution coupled climate runoff simulations of

547   seasonal snowfall over Colorado: a process study of current and warmer climate. J Climate

548   24:3015-3048. DOI:10.1175/2010JCLI3985.1.

549   Reich P B, Hobbie S E, Lee T D (2014) Plant growth enhancement by elevated CO_2 eliminated by

550   joint water and nitrogen limitation. Nature Geoscience 7, 920–924. DOI: 10.1038/ngeo2284.

551   Russell G, Wilson G W (1994) An Agri-Pedo-Climatological Knowledge-base of Wheat in Europe.

552   Joint Research Centre, European Commission, Luxembourg, CL-NA-15789-EN-C, pp. 158.

553   Schär C, Frei C, Lüthi D, Davies H C (1996) Surrogate climate-change scenarios for regional climate

554   models. Geophys Res Lett 23:669-672. DOI: 10.1029/96GL00265.

555   Semenov MA, Porter JR (1995) Climatic variability and the modelling of crop yields. Agr Forest

556   Meteorol 73:265–283. DOI: 10.1016/0168-1923(94)05078-K.

557   Smith N G, Dukes J S (2013) Plant respiration and photosynthesis in global-scale models:

558   incorporating acclimation to temperature and CO_2. Global Change Biology 19, 45–63. DOI:

559   10.1111/j.1365-2486.2012.02797.x.

560   Tao F, Zhang Z (2013) Climate Change, wheat productivity and water use in the North China Plain: A

561   new super ensemble-based probabilistic projection. Agr Forest Meteorol 170: 146-165.

562   DOI:10.1016/j.agrformet.2011.10.003.

563   Teixeira EI, Fischer G, van Velthuizen H, Walter C, Ewert F (2013) Global hot-spots of heat stress on

564   agricultural crops due to climate change. Agr Forest Meteorol 170:206-215.

565   DOI:10.1007/s10584-006-9051-4.

566   Tian Z, Zhong H, Shi R, Sun L, Fischer G, Liang Z (2012) Estimating potential yield of wheat

567   production in China based on cross-scale data-model fusion. Front Earth Sci 6:364-372.

568   DOI:10.1007/s11707-012-0332-0.

569   Timsina J, Humphreys E (2006) Performance of CERES-Rice and CERES-Wheat models in

570   rice–wheat systems: A review. Agricultural Systems, 90(1): 5-31.

571   DOI:10.1016/j.agsy.2005.11.007.

572   Trnka M, Rötter RP, Ruiz-Ramos M, et al. (2014) Adverse weather conditions for European wheat

573   production will become more frequent with climate change. Nature Climate Change 4:637–643.

574   DOI:10.1038/NCLIMATE2242.

575   Tubiello, FN, Donatelli M, Rosenzweig C, and Stockle CO (2000) Effects of climate change and

576   elevated CO2 on cropping systems: Model predictions at two Italian locations. Eur. J. Agron.

577   12:179-189.

578   USDA (2006) Wheat Situation and Outlook Yearbook. WHS-2006. Available at http://ers.usda.gov.

579   USDA (2016) World Agricultural Production. Circular Series WAP 7-16. Available at

580   http://usda.mannlib.cornell.edu/usda/current/worldag-production/worldag-production-07-12-2016.

581   pdf.

582   van Vuuren DP, Edmonds J, Kainuma M, et al. (2011) The representative concentration pathways: an

583   overview. Climatic Change, 109:5-31. DOI:10.1007/s10584-011-0148-z.

584   Váry Z, Mullins E, McElwain JC, Doohan FC (2015) The severity of wheat diseases increases when

585   plants and pathogens are acclimatized to elevated carbon dioxide. Global Change Biology. Early

586   online. DOI: 10.1111/gcb.12899.

587   Xiong W, Conway D, Holman I, Lin E (2008) Evaluation of CERES-Wheat simulation of wheat

588   production in China. Agron J 100:1720-1728. DOI:10.2134/agronj2008.0081.

589   Xiong W, Holman I, Lin E, et al. (2010) Climate change, water availability and future cereal

590   production in China. Agr Ecosyst Environ 135:58-69. DOI:10.1016/j.agee.2009.08.015.

591   Yadav SS, Redden R, Hatfield JL, Lotze-Campen H, Hall AJ (2011) Crop Adaptation to Climate

592   Change. John Wiley & Sons, Inc.

593   Yoshikane T, Kimura F, Kawase H, Nozawa T (2012) Verification of the Performance of the

594   Pseudo-Global-Warming Method for Future Climate Changes during June in East Asia. SOLA

595   8:133-136. DOI:10.2151/sola.2012-033.

596   You L, Rosegrant MW, Wood S, Sun D (2009) Impact of growing season temperature on wheat

597   productivity   in   China.   Agr   Forest   Meteorol,   149,   1009–1014.   DOI:

598   http://dx.doi.org/10.1016/j.agrformet.2008.12.004.

599

600

601 Table 1. Changes in the frequency of heat stress relative to the baseline (in days/decade)

Station	2016-2025		2045-2055		2091-2100	
	Pre-anthesis	Grain-filling	Pre-anthesis	Grain-filling	Pre-anthesis	Grain-filling
Winter wheat station						
Tacheng (TC)	21.8	11.4	28.8	20.4	40.6	35.4
Ruoqiang (RQ)	70.7	63.7	85.4	82	102.9	102.1
Tongzhou (TZ)	4.3	5.8	8.0	10.3	15.5	19.4
Linfen (LF)	14.5	6.1	20.1	11.4	29.8	21.8
Taigu (TG)	8.2	4.3	14.1	9.5	24.5	20.7
Jinghai (JH)	4.9	2.1	8.7	4.6	16.7	10.9
Tai-an (TA)	2.3	0.5	4.1	1.5	8.6	5.3
Dingxian (DN)	7.6	8.5	12.8	14.9	21.4	26.8
Linyi (LY)	7.2	4.5	12.6	7.1	20.6	10.3
Wugong (WG)	12.4	8.9	16.1	12.3	22.1	13.6
Xuzhou (XZ)	4.6	1	6.8	2.6	11.5	6.7
Tianshui (TS)	17	2.4	23.9	5	34.4	12.9
Lasa (LS)	0.8	0.1	2.5	0.5	10.3	0.8
Zhumadian (ZM)	4.0	4.2	6.1	5.8	10.7	11.2
Kashi (KS)	12.2	5.4	21.5	13.6	37	29.7
Nangong (NG)	11.5	9.4	17.5	12.8	29.1	18.2
Zhengzhou (ZZ)	10.8	3.1	15.5	4.3	18.8	9.2
Pu-an (PA)	6.9	3.6	11	6.1	17.9	15.5
Hefei (HF)	2.4	2.8	4.2	5.3	8.5	8.9
Kunming (KM)	0.5	0.1	1.0	0.1	3.1	1.0
Baoshan (BS)	0.2	0.1	0.3	0.1	0.5	0.4
Wenjiang (WJ)	0.5	0.7	1.1	1.2	3.4	3.5
Songjiang (SJ)	0.1	0.2	0.6	1	1.8	2.8
Macheng (MC)	1.5	2.1	3.4	3.7	7.6	8.7
Jiangjin (JJ)	0.3	1.7	0.7	2.8	2.4	6.1
Longhai (LH)	0.2	0.1	0.3	0.1	0.5	0.1
Spring wheat station						
Jiuquan (JQ)	30.8	7.0	36	13.9	49.3	24.4
Tulufan (TL)	91.7	105.1	107	122.3	120.8	136.2
Dunhuang (DH)	56.1	46.9	73.5	70.5	92.3	92.4
Dingxi (DX)	0.4	0.1	1.2	0.6	8.3	5.2
Guyuan (GN)	1.4	0.0	4.6	0.6	12.9	6.7
Huangyuan (HY)	0.2	2.1	1.4	4.6	8.5	9.7
Guyang (GY)	74.6	29.2	93.5	42	114.8	63.6
Aletai (AL)	43.6	7.7	58.5	16.2	72.5	28.4
Zhangbei (ZB)	6.7	1.4	12.8	3.5	24.4	9.2
Huma (HM)	27.7	18.7	39.6	26.6	55.2	40.4

602 Note: Specific to this research, pre-anthesis period spans from the 20th day before anthesis to the anthesis day,

603 and grain-filling period spans from the 1st to 20th day after anthesis.

604

605

606   Table 2. Ensemble mean yield changes, probability of yield loss, and standard deviation (S.D.)

607   of yield change relative to the baseline and under irrigated condition

	2016-2025		2045-2055		2091-2100	
Station	Mean yield change in % (Probability in %)	S.D. in kg/ha (as % of baseline yield)	Mean yield change in % (Probability in %)	S.D. in kg/ha (as % of baseline yield)	Mean yield change in % (Probability in %)	S.D. in kg/ha (as % of baseline yield)
Winter wheat station						
Tacheng	-7.4 (80.6)	447.3 (7.7)	-8.2 (80.6)	484.6 (8.4)	-7.9 (74.6)	627.9 (10.9)
Ruoqiang	-3.6 (94.0)	144.0 (2.6)	-3.2 (94.0)	231.5 (4.2)	-5.1 (91.0)	379.9 (7.0)
Tongzhou	-2.8 (71.6)	424.1 (6.1)	-5.8 (58.2)	441.6 (6.3)	-8.3 (70.1)	581.2 (8.3)
Linfen	-2.8 (68.7)	302.0 (5.2)	-5.6 (85.1)	302.1 (5.2)	-9.2 (92.5)	426.5 (7.4)
Taigu	-6.5 (86.6)	325.5 (5.5)	-2.2 (61.2)	321.4 (5.4)	-3.1 (68.7)	337.7 (5.7)
Jinghai	-6.0 (88.1)	280.3 (5.2)	-3.5 (73.1)	278.1 (5.2)	-5.5 (76.1)	404.3 (7.6)
Taian	-4.0 (88.1)	218.7 (3.4)	-3.1 (82.1)	234.7 (3.6)	-5.2 (82.1)	375.6 (5.8)
Dingxian	-8.9 (82.1)	349.4 (8.9)	-12.4 (92.5)	437.5 (11.1)	-16.2 (83.6)	610.1 (15.5)
Linyi	-3.0 (67.2)	509.4 (10.1)	8.2 (70.9)	500.8 (9.9)	13.6 (80.4)	568.6 (11.3)
Wugong	-3.7 (61.9)	330.0 (6.9)	-7.9 (69.2)	315.5 (6.6)	-10.8 (71.4)	501.7 (10.5)
Xuzhou	-6.2 (94.0)	274.4 (3.8)	-7.6 (91.0)	333.4 (4.6)	-8.2 (91.0)	494.7 (6.8)
Tianshui	-10.7 (92.5)	384.8 (7.8)	-12.1 (91.0)	514.5 (10.4)	-15.0 (85.1)	638.9 (12.9)
Lasa	-8.3 (100.0)	359.3 (3.7)	-7.6 (94.0)	466.3 (4.7)	-9.2 (97.0)	557.6 (5.7)
Zhumadian	-3.8 (88.1)	283.4 (6.0)	-4.9 (88.1)	412.2 (8.8)	-8.5 (80.6)	429.9 (9.1)
Kashi	-5.4 (85.1)	415.3 (6.9)	-6.3 (88.1)	369.5 (6.2)	-9.4 (97.0)	414.4 (6.9)
Nangong	-5.8 (78.1)	210.4 (4.0)	-7.5 (83.3)	245.7 (4.7)	-9.6 (95.2)	381.2 (7.2)
Zhengzhou	-4.7 (70.5)	255.6 (4.9)	-7.5 (77.8)	273.6 (5.3)	-9.2 (82.4)	501.7 (9.6)
Puan	-1.9 (58.2)	335.1 (7.5)	-1.9 (56.7)	302.7 (6.8)	-4.3 (68.7)	372.6 (8.3)
Hefei	-0.7 (58.2)	524.2 (7.1)	-2.1 (69.9)	414.9 (5.7)	-6.1 (70.3)	603.7 (8.2)
Kunming	-4.6 (80.6)	426.7 (5.4)	-5.0 (83.6)	387.3 (4.9)	-4.2 (77.6)	541.1 (6.8)
Baoshan	-1.5 (53.7)	302.9 (4.6)	-4.7 (89.6)	255.8 (3.9)	-7.2 (88.1)	432.4 (6.6)
Wenjiang	-3.7 (80.6)	471.3 (7.0)	-4.3 (80.6)	459.8 (6.9)	-5.8 (65.7)	549.7 (8.2)
Songjiang	-3.1 (85.1)	310.5 (7.1)	-4.9 (79.1)	256.9 (5.9)	-5.2 (68.7)	387.3 (8.9)
Macheng	-3.4 (94.0)	313.5 (5.1)	-7.0 (91.0)	388.9 (6.3)	-9.8 (79.1)	499.4 (8.1)
Jiangjin	-5.6 (62.7)	586.0 (18.1)	-7.6 (34.3)	642.8 (19.8)	-10.9 (32.8)	851.3 (26.3)
Longhai	-3.1 (68.7)	306.8 (11.4)	-4.2 (67.2)	342.2 (12.7)	-4.9 (56.7)	529.9 (19.7)
Spring wheat station						
Jiuquan	-9.1 (92.5)	269.1 (5.4)	-15.3 (95.2)	452.9 (15.9)	-19.5 (98.4)	843.6 (29.6)
Tulufan	-12.4 (92.5)	201.3 (8.9)	-23.3 (98.5)	273.2 (12.0)	-33.6 (98.5)	489.9 (21.6)
Dunhuang	-5.4 (89.6)	209.7 (4.9)	-10.7 (98.5)	339.0 (8.0)	-15.2 (94.0)	572.1 (13.5)
Dingxi	-3.1 (79.1)	86.7 (3.6)	-4.8 (83.6)	105.3 (4.4)	-7.4 (88.1)	174.2 (7.2)
Guyuan	-4.1 (89.6)	116.6 (4.1)	-6.6 (98.5)	114.9 (4.0)	-9.3 (95.5)	186.7 (6.5)
Huangyuan	-6.0 (95.5)	193.2 (3.4)	-9.4 (100.0)	254.0 (4.5)	-12.0 (98.5)	397.5 (7.0)
Guyang	-12.5 (100.0)	62.6 (3.8)	-18.5 (100.0)	109.5 (6.6)	-24.2 (100.0)	236.1 (14.3)
Aletai	-10.7 (95.2)	321.7 (8.2)	-19.2 (96.7)	484.1 (12.4)	-25.6 (98.4)	745.2 (19.1)
Zhangbei	-8.9 (100.0)	175.1 (4.1)	-9.1 (97.0)	199.2 (4.7)	-12.9 (97.0)	386.3 (9.0)
Huma	-9.9 (98.5)	121.4 (5.4)	-11.1 (97.0)	133.9 (6.0)	-15.7 (95.5)	249.9 (11.2)

608

609
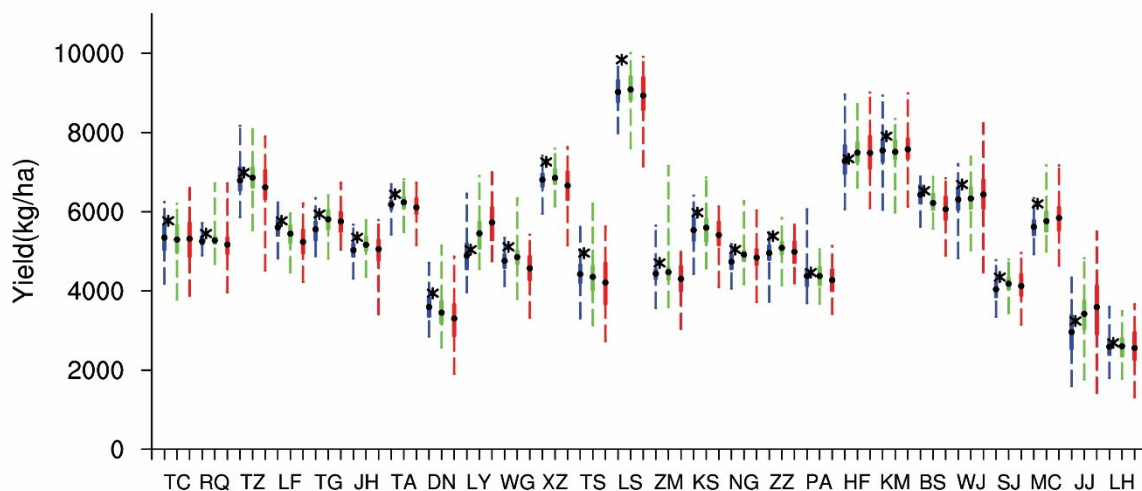
610
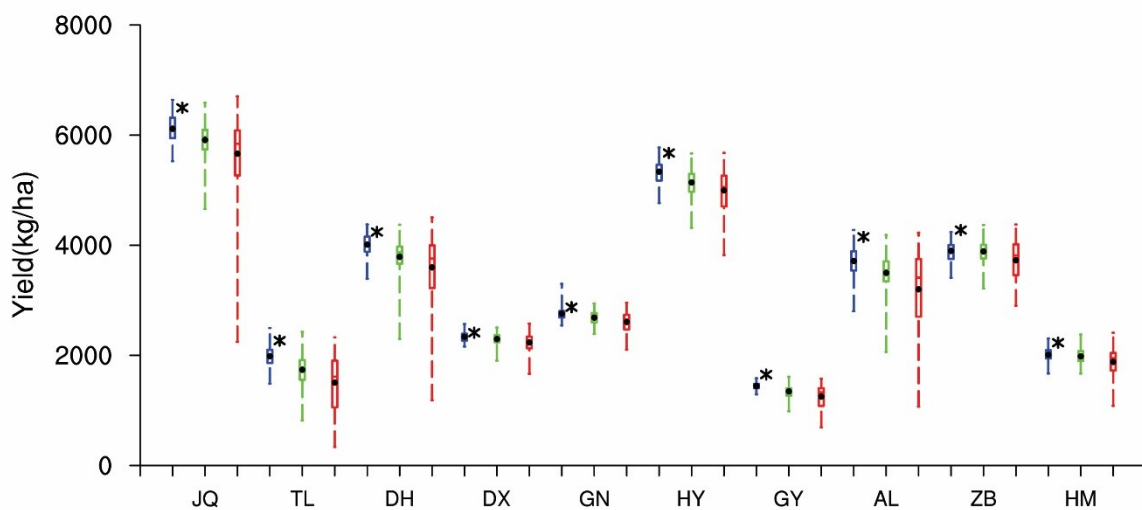
611

612 Fig.1 The ensemble yields of irrigated winter wheat (upper panel) and spring wheat (lower
613 panel) in early (blue), middle (green), and the end (red) of the 21st century. The asterisk
614 represents the 10–year average irrigated wheat yield from 1996 to 2005 simulated with the
615 observation data as the baseline. The dot denotes the ensemble mean.

616

617